Turbulent Combustion in Piston Engines driven by Sewage Gas for the Cogeneration of Heat and Power

LUCAS KONSTANTINOFF[1], DOMINIK MAIREGGER[2],CHRISTOPH PFEIFER[3], UWE TRATTNIG[4], THOMAS DORNAUER[1], LUKAS MÖLTNER[1]
[1]Department of Technology and Life Sciences
Management Center Innsbruck (MCI)
Universitätsstraße 15, 6020 Innsbruck, AUSTRIA
lukas.moeltner@mci.edu http://www.mci.edu
[2]Professional Gas Engine Solutions GmbH (PGES), AUSTRIA
[3] Institute for Chemical- and Energy Engineering, Universität der Bodenkultur (BOKU), Vienna, AUSTRIA
[4]Energy and Transport Management, FH Joanneum, Kapfenberg, AUSTRIA

Abstract: In this study, the influence of the charge motion on the internal combustion in a sewage gas driven engine (150 kW) for combined heat and power units was investigated. For this purpose, the geometry of the combustion chamber in the immediate vicinity to the valve seats was modified. The geometrical modification measures were conducted iteratively by integrative determination of the swirl motion on a flow bench and consecutively by combustion analysis on a test engine. Two different versions of cylinder heads were characterized by dimensionless flow and swirl numbers prior to testing their on-engine performance. Combustion analysis was conducted with a cylinder pressure indication system for partial and full load, meeting the mandatory NO_x limit of 500 $mg \cdot m^{-3}$. Subsuming the flow bench results, the new valve seat design has a significant enhancing impact on the swirl motion but also leads to disadvantages concerning the flow rate. A comparative consideration of the combustion rate shows that the increased swirl motion results in faster combustion and hence in higher efficiency. In summary, the geometrical modifications close to the valve seat result in increased turbulence intensity, and it was proven that this intensification raises the ratio of efficiency by 1.6%.

Key-words: Combined heat and power, biogas, turbulent combustion, charge motion

1 Introduction

Reciprocating piston engines are one of the most effective and reliable options to convert burnable gases to electric power and heat energy. Biogas and other methane-containing gases (e.g., sewage gas) have gained importance due to better knocking-resistance, favorable combustion characteristics and lower overall CO_2 emissions feature advantages compared to conventional fuels as natural gas. The demand for efficient internal combustion engines (ICEs) able to meet current and future global emission legislations motivates recent research and development activities [1].

The utilization of non-fossil gases with varying compositions and real-life operation conditions, including partial load operation, necessitates adaptations for ICEs to ensure the highest possible efficiency regarding CO_2- and NO_x- emissions [2,3].

A comparably simple yet effective method to improve an engine's efficiency is to optimize in-cylinder flow characteristics, which are mainly influenced by the combustion-chamber design (e.g., cylinder head, valve seat, inlet port geometry and piston) [4,5]. In combination with highly accurate adjustments of engines' control parameters (e.g., ignition timing (IT), ignition duration (ID), boost pressure and air/fuel-ratio (λ)), high-turbulence intensities have the potential to increase efficiency significantly [6,7].

Fundamental knowledge of the relation between component geometries and their flow characteristics and combustion performance, particularly during varying load scenarios, is substantial for the design and development of advanced engine components.

Hence, the goal of the present research was to investigate the implications of new valve-seat geometries on volumetric efficiency and internal combustion in a state-of-the-art biogas ICE of a combined heat and power unit (CHP) [8].

2 State of the Art

2.1 Internal Combustion

In almost every internal-combustion process, combustion velocity is strongly influenced by the surrounding turbulence fields. Both the kinetic energy of turbulence and size of occurring eddies

have a significant influence on the progress of combustion and the combustion rate.

There are two distinguished types of combustion: deflagration and detonation. Typical characteristics of deflagration are flame propagations, which are controlled either by reaction rates of occurring chemical reactions or limitations caused by transport phenomena. For both, the velocity of the flame front is smaller than sonic speed. Fig. 1 illustrates three different combustion regimes of deflagration caused by different intensities of turbulence [9]. Low turbulence intensity results in an enclosed propagation of a filmy flame front with laminar flame velocity V_l, depicted in fig. 1 a). Increasing turbulence leads to a convolution of the flame front and the formation of single flamelets. The flame front remains enclosed and moves with the turbulent velocity V_t, as shown in fig. 1 b). If the turbulences' intensity is further increased, the flame front disintegrates into a homogeneous admixture of already burnt and unburnt gases (= ideal stirred reactor) and presents the highest combustion rates. Subsuming the velocity of the flame propagation and thus the combustion rate are strongly influenced by the turbulence inside the combustion chamber [10,11].

In contrast to combustion processes caused by deflagration, the characteristics of detonations show multiply higher velocities of the flame front (> 1000 m/s) and flame propagation promoted by a pressure wave maintained by chemical reactions and thus by the heat release of the combustion [12,13,14].

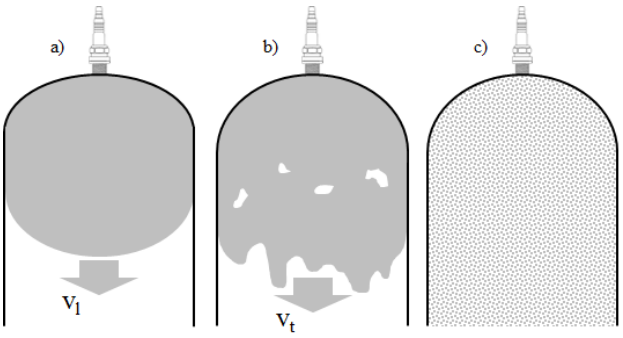

Fig. 1: Types of flame propagation with respect to the intensity of turbulence

2.2 Thermodynamic Background

From a thermodynamic standpoint, internal combustion should occur infinitely fast so that all of the heat released can be utilized to increase the temperature inside the combustion chamber. The more time needed for combustion, the more energy is consumed for volume work during the expansion stroke.

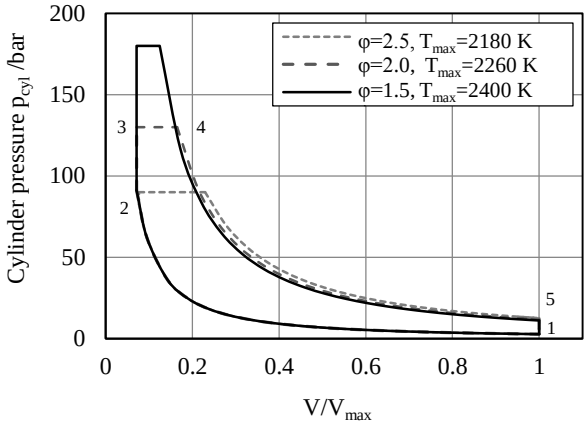

Fig. 2: Simplified Seiliger-cycle for the test engine for volume ratios (V4/V3) of φ = 1.5, φ = 2, φ = 2.5 and maximum temperatures; compression ratio ε = 14, boost pressure p_{boost} = 1.54 bar, c_p = 1004 J·(kgK)$^{-1}$, c_v = 717 J·(kgK)$^{-1}$, Q_{in} total = 8000 J

This fact results consequently in a reduced maximum working temperature and hence in a lower ratio of efficiency [15]. Fig. 2 explains the principle of the advantageous turbulent combustion concept strongly simplified by the Seiliger cycle. For improved comparability, the engine parameters used for these calculations were chosen in accordance with the test engine shown in table 1.

Fig. 3 presents the implications of the considered volume ratios φ with respect to thermal efficiency. A comparison between fig. 2 and fig. 3 illustrates that faster combustion, which can be identified by a low volume ratio φ, increases the maximum working temperature and thus the thermal ratio of efficiency [15]. Therefore, a target-orientated optimization of the charge motion inside the combustion chamber has the potential to increase the engine's efficiency.

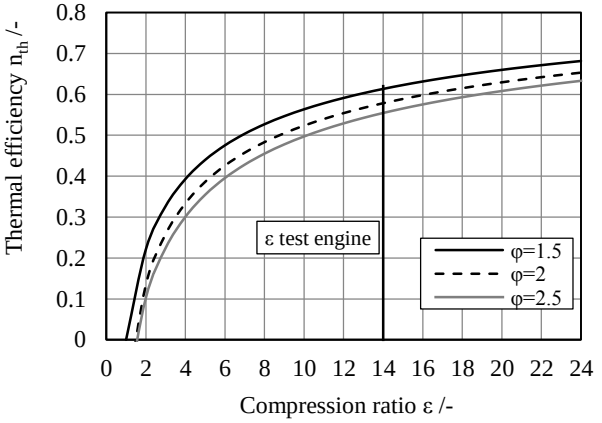

Fig. 3: Potential gain in efficiency with optimized burning velocities

2.3 Charge Motion

The charge motion in the combustion chamber is the strongest determinant for mass transfer during internal combustion and heat dissipation via the cylinder wall, cylinder head and piston. The charge motion can be classified into three primary types: swirl-, tumble- and squish flows [16].

The first flow-type, the swirl flow, is a radial rotating motion of inflowing gas that can be provoked either by a tangential geometry of the inlet channel or by the geometry next to the valve seat. It has been reported that geometric measures in the vicinity of the valve seat have the potential to increase swirl, particularly at small valve lifts [17].

Contrary to the swirl flow, the tumble describes a rotating charge motion in a vertical direction that can be induced by the inlet geometry and/or shape of the piston head. The effect of tumble is only available as long as the piston is not moving upwards, hence in early stages of loading.

Squish flows are the product of displacement effects between the combustion chamber and upward-moving piston. Squish flows are only of importance close to top dead center (TDC) and result in a high heat release at an early stage of combustion [18].

3 Methodology and Experimental Set Up

3.1 Test Engine and Cylinder Heads

A state-of-the-art biogas cogeneration unit with a nominal power output of 150 kW (P_{ISO}) was used for this research. The test engine was connected to the municipal heat and electricity grids, providing a real-life test-engine set-up. Table 1 shows relevant technical engine specifications.

The newly designed *HiGas* cylinder head features no differences in inlet manifold geometry compared to the baseline version. However, it deviates near the inlet valve seats, where sickle-shaped cuts have been made to change the flow pattern.

Fig. 4 is a comparative depiction of the baseline cylinder head (left) and the newly developed *HiGas* model (right).

Table 1: Technical specifications of the test engine

ISO standard power (mech.)	P_{ISO}	/kW	150
Air/fuel ratio	λ	/-	1.55
Compression ratio	ε	/-	14:1
Brake mean effective pressure	BMEP	/bar	15.8
Electrical efficiency	η_{el}	/%	40.2
Mechanical efficiency	η_{mech}	/%	42.2
Number of cylinders		/-	4

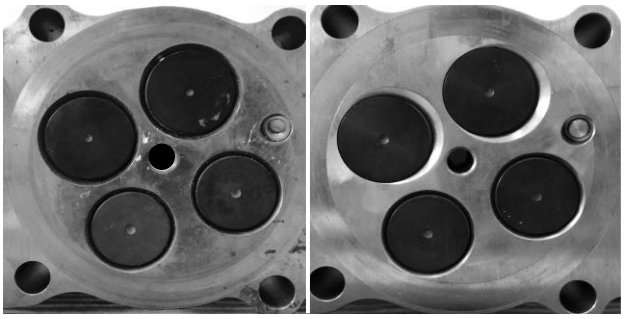

Fig. 4: Baseline and new HiGas cylinder head with sickle-shaped cuts near the inlet valves' seats

It reveals that the sickle shape near the first inlet valve of the *HiGas* cylinder head is directed towards the second inlet valve and spark plug, and the second sickle shape is targeted tangential to the wall to enhance rotational gas movement.

3.2 Experiments on the Static Flow Bench

To allow examination of the different cylinder head versions, a static flow bench was designed and constructed at *MCI* Innsbruck, fig. 5. The air flow and its angular momentum, which is generated by the sickle-shaped cut and inlet port of the cylinder head, were measured at different valve lifts. In accordance with the integrative method *Tippelmann* described, a torque meter was used to capture the complete rotational motion of the flow pattern [19,20,21].

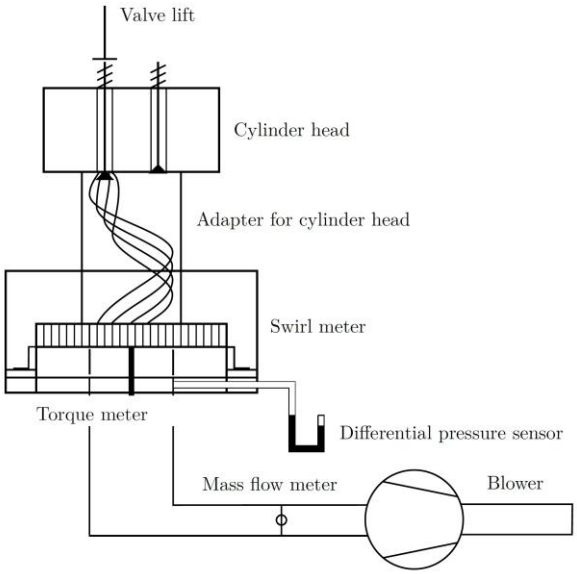

Fig. 5: Schematic overview of the constructed static flow bench

When intake air flows through a low-friction mounted flow rectifier connected to a torque meter, the angular momentum of the intaken air is transferred to the torque meter and quantified.

Flow and swirl coefficients were calculated using the information received on flow and torque.

The measured torque M equals the initial impulse $\dot{I}$ of the air flow by assuming a frictionless bearing of the flow rectifier and a fully rectified air flow. *Tippelmann* defines the torque as being proportional to the square of the volumetric flow rate $\dot{V}$ and the density ρ of air.

$$M = \dot{I} = D^* \cdot \dot{V}^2 \cdot \rho \quad (1)$$

The factor D^* describes the relationship between the swirl number K_S and the cylinder diameter d_{cyl}.

$$D^* = \frac{2 \cdot K_S}{d_{cyl}} \quad (2)$$

Combining and rearranging (1) and (2) delivers the swirl coefficient, equation (3).

$$K_S = \frac{M \cdot \rho \cdot d_{cyl}}{2 \cdot \dot{m}^2} \quad (3)$$

The thermal equation of state is used to determine the density of dry air, equation (4).

$$\rho = \frac{p}{R_s \cdot T} \quad (4)$$

The pressure, which is needed to calculate the density of dry air, is derived from the difference between the atmospheric pressure p_0 and the pressure drop through the swirl meter that was kept constantly at $\Delta p = 50$ mbar. As a result, the swirl number K_S can be calculated from the measured data, equation (5).

$$K_S = \frac{M \cdot (p_0 - \Delta p) \cdot d_{cyl}}{2 \cdot \dot{m}^2 \cdot R_S \cdot T} \quad (5)$$

With the mass flow rate also being recorded at the static flow bench, two flow coefficients can be determined. The flow coefficient $\mu\sigma$ is related to the valve-seat diameter and gives information about the inlet-port quality. The flow coefficient α_k is related to the bore diameter and allows a comparison of different cylinder heads' overall flow performance. The flow coefficients are both defined as a ratio of the measured flow rate $\dot{m}$ to the theoretical flow rate $\dot{m}_{th,Valve/Bore}$ with respect to the applicable geometric reference, equations (6) and (7).

$$\mu\sigma = \frac{\dot{m}}{\dot{m}_{th,Valve}} \quad (6)$$

$$\alpha_k = \frac{\dot{m}}{\dot{m}_{th,Bore}} \quad (7)$$

The theoretical flow rate $\dot{m}_{th}$, for both valve and bore diameter reference, is calculated using equation (8) [22].

$$\dot{m}_{th,Valve/Bore} = A_{Valve/Bore} \cdot \rho_{Air,m} \cdot \sqrt{\frac{2 \cdot p_0}{\rho_{Air,m}}} \cdot \sqrt{\frac{\kappa}{(\kappa - 1)}} \cdot \sqrt{\left(1 - \frac{p_1}{p_0}\right)^{\frac{2}{\kappa}} - \left(1 - \frac{p_1}{p_0}\right)^{\frac{\kappa+1}{\kappa}}} \quad (8)$$

Here, A_{Valve} and A_{Bore} are the related geometric references. An isentropic exponent of $\kappa = 1.4$ is used for air at 20°C. The density of the moist air around the flow bench $\rho_{Air,m}$ and the static pressure inside the vessel p_1 were derived from recorded data.

With these calculations, the characterization of the respective cylinder heads was enabled. Because increased swirl can result in lower flow rates, both swirl and flow numbers must be examined to evaluate the influence of valve-seat design and inlet-port quality on flow rates and swirl.

3.3 Experiments on the Engine Test Bench

The test-engine set-up is schematically shown in fig. 6. The applied test engine is driven by sewage gas and equipped with an *AVL* indication system that records the cylinder pressure over the crank angle. The indication system used for data acquisition is the compact combustion-measurement system *INDIMICRO*. The software used to process the data was *INDICOM* version *2.7*. A calculation of the heat released by means of the recorded cylinder pressure was conducted. Hence, overall engine performance was monitored and evaluated for different load conditions. The results were acquired by averaging data of 200 recorded cycles for each measured load. The electricity produced by the generator and fuel consumption were measured for a certain amount of time once the engine reached steady state at a set load.

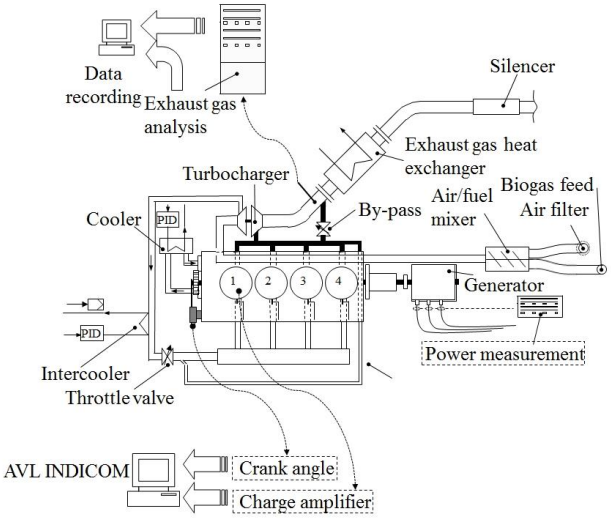

Fig. 6: Scheme of experimental set-up

Table 2 shows the results of the engine calibration during the test runs. The set loads were at 100%, 75% and 50% of the engine's nominal power output of 150 kW. The firing point was kept constant at 22° TDC. The air/fuel ratio was controlled to meet the NO_x emission regulations of 500 mg·m^{-3}.

Table 2: Calibration of the cogeneration unit during the test runs

Set load /kW	150	112	75
Ignition timing/ °CA ATDC		-22	
λ HiGas	1.644	1.580	1.530
λ Baseline	1.643	1.610	1.532
NO_x HiGas /mg·m^{-3}	499	547	520
NO_x Baseline /mg·m^{-3}	494	490	542

The sewage gas used was produced onsite at the wastewater purification plant. It consisted of 57.3% methane with a calorific value of 5.75 kWh·m^{-3}. The respective values can be seen in table 3.

Table 3: Methane content and calorific heat value of the applied sewage gas during the testing

Set load /kW	150	112	75
Methane HiGas /%	57.3	57.3	57.3
Methane Baseline /%	57.7	57.3	57.3
Calorific value HiGas /kWh·m^{-3}	5.74	5.74	5.74
Calorific value Baseline /kWh·m^{-3}	5.76	5.80	5.80

4 Results and Discussion

4.1 Static Measurements

The two cylinder heads are examined and compared regarding their flow and swirl coefficients and on-engine performances. Fig. 7 reveals that modifying the geometry near the valve seat has a strong influence on the swirl, particularly at low valve lifts, when exiting air has high velocity and the flow passing the sickle-shape is forced into a rotational motion. At a valve lift of approximately 8 mm, the swirl flow breaks down, and the tangential motion of the flow pattern changes into a flow with axial direction to the cylinder axis. With further opening of the valve, decreasing velocity reduces the force with which the air is directed toward the sickle shape so that swirl drops to the level of the baseline cylinder head. Swirl is then only generated by the arrangement and design of the intake manifolds of the cylinder heads. Because the cylinder heads only differ by the valve-seat design, the swirl reaches the same level once the effect of the sickle shape wears off. The point when the valve-seat design's effect is insignificant can be seen at a valve lift of $h_v > 8$ mm.

The flow coefficient of the non-swirl baseline cylinder head is slightly above the flow coefficient of the *HiGas* cylinder head, as swirl leads to increased pressure loss. As both cylinder heads have the same inlet manifold geometry, α_k is used to provide evaluation criteria on global flow performance of the cylinder heads. The flow coefficient α_k in relation to the valve lift is depicted in fig. 8. In the case of small valve lifts, the relatively small cross intersection between the valve disc and seat restrict the air flow for both cylinder head variants. This effect is stronger for the HiGas-cylinder head with its sickle shape due to the redirection of the flow pattern, resulting in higher pressure drops.

To summarize, two effects could be determined that show the potential to influence combustion contrarily. On the one hand, the swirl coefficient is expected to increase combustion rates due to higher turbulence intensity; on the other hand, rising swirl reduces volumetric efficiency expressed by lower flow coefficients.

The consecutive combustion analysis allows a holistic evaluation of both effects influencing the internal combustion.

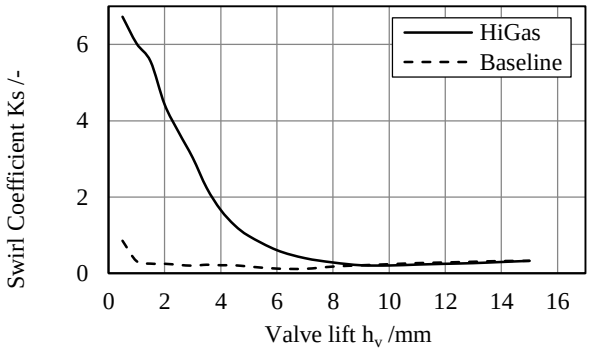

Fig. 7: Comparison of the swirl number Ks

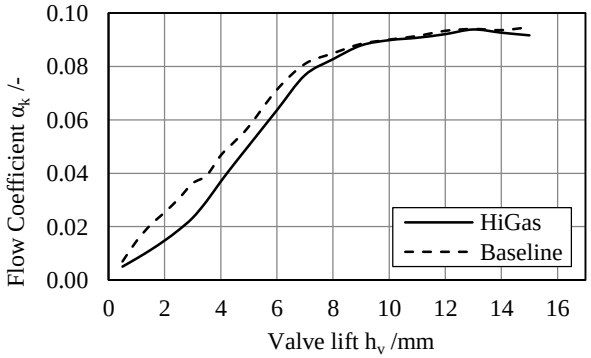

Fig. 8: Comparison of the flow number α_k

4.2 Combustion analysis

Fig. 9 shows the indicated cylinder pressure in relation to the crank angle (CA) at different load conditions. The generated swirl motion proves to overcompensate the abovementioned reduced

volumetric efficiency by showing higher peak pressures. The peak pressure achieved at a full-load condition differs by as much as 20 bars, showing the maximum impact during this study. At partial load, the cylinder pressures are increased as well but to a lower extent compared to full load operation. These results strongly correspond to the thermodynamic background expressed in the introduction of this study.

The burning process of the test engine is expressed by the combustion rate (AQ_i) that shows at which crank angle what percentage of heat has been released (fig. 10). The curve shows the ignition delay (IGD), which describes the time period between the firing point (FP) at 22° BTDC and the start of combustion $AQ_{5\%}$, the center of combustion $AQ_{50\%}$ and the end of combustion $AQ_{90\%}$.

At a constant firing point, an earlier crank angle of $AQ_{50\%}$ is equal to a faster burning velocity, as it is reached at an earlier timestamp.

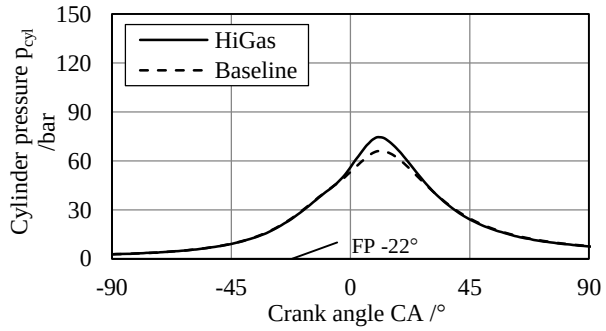

(a) Cylinder pressure at 75 kW load

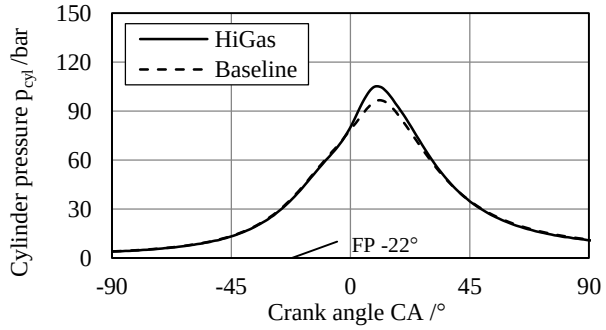

(b) Cylinder pressure at 112 kW load

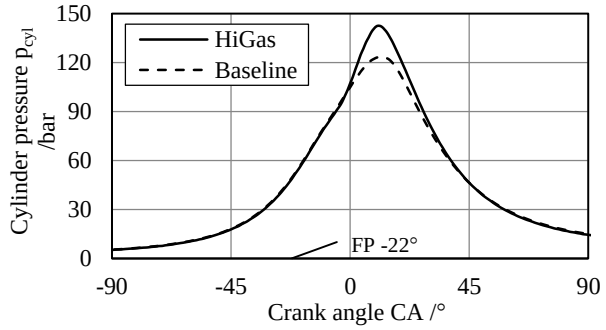

(c) Cylinder pressure at 150 kW load

Fig. 9: Cylinder pressure over crank angle at different loads (a-c)

To improve comparability, the positions of the $AQ_{50\%}$ values are listed in table 4.

The results show a significantly faster combustion at otherwise constant engine parameters. At full load operation (150 kW), the maximum reduction of burning duration ($AQ_{5\%}$ until $AQ_{90\%}$) is 11.7° CA; at partial load, reduced combustion duration can be seen as well.

Fig. 11 gives an overview of all combustion parameters for both cylinder head variants and all considered load scenarios. It is notable that burning velocity is nearly equally high for each load condition using the new *HiGas* cylinder head. IGD and $AQ_{50\%}$ is reached at a similar level independent of the set load. The sickle-shaped valve seats influence the IGD and furthermore the position of $AQ_{50\%}$ and total burning duration.

The burning duration of the baseline cylinder head strongly depends on the set load, whereas the new *HiGas* cylinder head is not affected by

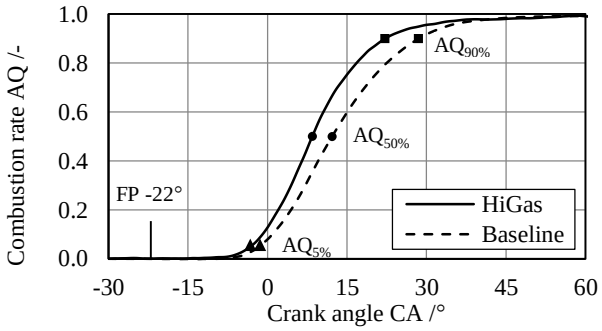

(a) Combustion rate at 75 kW load

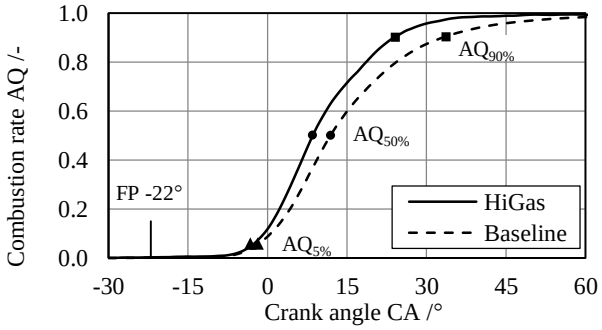

(b) Combustion rate at 112 kW load

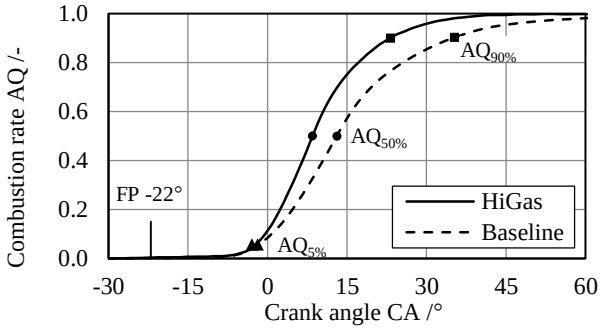

(c) Combustion rate at 150 kW load

Fig. 10: Combustion rate over crank angle at different loads (a-c). Relevant points of AQ_i drawn into the curves.

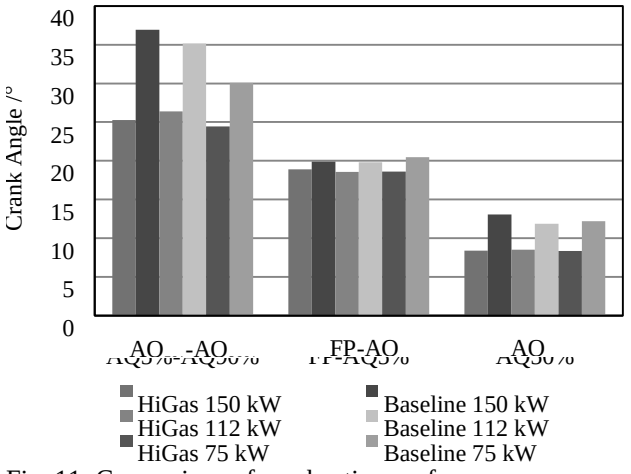

Fig. 11: Comparison of combustion performance

fluctuating load conditions.

Considering the electrical efficiency of the cogeneration unit, an increase of up to 1.59% was achieved with usage of the *HiGas* cylinder head with sickle-shaped valve seats. At full and partial loads, the gain in efficiency is significant; at a low partial load operation, only a small increase was measured. With regard to theoretical assumptions, increasing electrical efficiency at low load conditions is expected to be achieved, although it was not measured.

Table 4: Comparison of electric efficiencies

Set load /kW	150	112	75
η_{el} HiGas /%	40.28	39.47	36.17
η_{el} Baseline /%	38.95	37.88	36.13
η_{el} Difference /%	1.33	1.59	0.04

5 Conclusion

Cylinder heads with two different valve-seat designs were tested on a static flow bench to acquire comparable data describing flow characteristics. Data on air-flow rate and angular momentum generated by the inlet port was used to calculate the flow and swirl coefficients describing the cylinder heads' static-flow performances. The benchmarked cylinder heads were mounted on a state-of-the-art biogas CHP unit, engine performance was measured and the combustion was analyzed with an indication system.

The sickle-shaped valve-seat design has a significant influence on the measured swirl, particularly at small valve lifts when air flow around the seat has a high velocity. Increased swirl reduces the volumetric efficiency, but the turbulence pattern has the potential of overcompensating for this disadvantage.

The strongly positive influence of the generated swirl on combustion characteristics was shown in all operation conditions. Through all loads, maximum cylinder pressure and correlating combustion rates were higher with the new valve-seat design. Additionally, overall combustion velocity seemed to not be affected by the load at which the engine was run. This means the new sickle-shape design is likely to improve burning velocities for all stationary-operated gas engines of similar size. Further research will include detailed consideration of partial load operation, particularly at 50% of the nominal power output. These already-planned experimental investigations are expected to show the degree of influence of the swirl motion on full- and partial-load operation.

In the course of this study, it was proven that a goal-orientated optimization of the charge motion has the potential to improve internal combustion and, hence, thermal efficiency.

Acknowledgements

This research project was funded as a cooperation and innovation project by the Tyrolean Government. The authors gratefully acknowledge all support the Tyrolean government and cooperating research partners PGES, ECI-M and MCI provided.

References:

[1] T. Shudo, T. Nagano and M. Kobayashi, Combustion Characteristics of Waste Pyrolysis Gases in an Internal Combustion Engine, International Journal of Automotive Technology, 4(1), 1-8, 2003.

[2] Kim, Yungjin; Kawahara, Nobuyuki; Tomita, Eiji; Oshibe, Hiroshi; Nishikawa, Koichi: Effect of Bio-Gas Contents on SI Combustion for a Co-Generation Engine. In: SAE Technical Paper Series, 2015, DOI: 10.4271/2015-01-1946.

[3] J. Yao-hua, et al., Research of Biogas as Fuel for Internal Combustion Engine, Power and Energy Engineering Conference, APPEEC 2009. Asia-Pacific. IEEE, pp. 1-4, 2009.

[4] P. G. Tewari, J. P. Subrahmanyam and M. K. Gajendra Babu, Experimental Investigations on the Performance Characteristics of a Producer Gas Fueled Spark Ignition Engine, SAE Paper No. 2001-01-1189, 2001

[5] Wheeler, J., Stein, J., and Hunter, G., Effects of Charge Motion, Compression Ratio, and Dilution on a Medium Duty Natural Gas Single Cylinder Research Engine, SAE Int. J. Engines 7(4):1650-1664, 2014, doi:10.4271/2014-01-2363.

[6] Abidin, Z., Hoag, K., Mckee, D., and Badain, N., "Port Design for Charge Motion Improvement within the Cylinder," SAE Technical Paper 2016-01-0600, 2016, doi:10.4271/2016-01-0600.

[7] Ogink, R. and Babajimopoulos, A., Investigating the Limits of Charge Motion and Combustion Duration in a High-Tumble Spark-Ignited Direct-Injection Engine, *SAE Int. J. Engines* 9(4):2129-2141, 2016, doi:10.4271/2016-01-2245.

[8] Porpatham, E.; Ramesh, A.; Nagalingam, B. (2013): Effect of swirl on the performance and combustion of a biogas fuelled spark ignition engine. In: Energy Conversion and Management 76, S. 463–471. DOI: 10.1016/j.enconman.2013.07.071.

[9] König, G.; Maly, R. R.; Bradley, D.; Lau, A. K. C.; Sheppard, C. G. W.: Role of Exothermic Centres on Knock Initiation and Knock Damage. In: SAE Technical Paper Series, 1990, DOI: 10.4271/902136.

[10] Wildman, C. and Cheng, W., The Effects of Charge Motion and Laminar Flame Speed on Late Robust Combustion in a Spark-Ignition Engine, *SAE Int. J. Engines* 3(1):202-213, 2010, doi:10.4271/2010-01-0350.

[11] Laget, O., Zaccardi, J., Gautrot, X., Mansion, T. et al., Establishing New Correlations Between In-Cylinder Charge Motion and Combustion Process in Gasoline Engines Through a Numerical DOE, SAE Int. J. Engines 3(1):183-201, 2010, doi:10.4271/2010-01-0349.

[12] Benson, G., Fletcher, E., Murphy, T., and Scherrer, H.: Knock (Detonation) Control by Engine Combustion Chamber Shape. SAE International Congress and Exposition ,1983. DOI: 10.4271/830509.

[13] McKenzie, J. and Cheng, W., The Anatomy of Knock, SAE Technical Paper 2016-01-0704, 2016, doi:10.4271/2016-01-0704.

[14] Piock, W., Befrui, B., Berndorfer, A., and Hoffmann, G., Fuel Pressure and Charge Motion Effects on GDi Engine Particulate Emissions, SAE Int. J. Engines 8(2):464-473, 2015, doi:10.4271/2015-01-0746.

[15] Pischinger, Rudolf; Klell, Manfred; Sams, Theodor (2009): Thermodynamik der Verbrennungskraftmaschine. 3. Aufl. Wien, New York, NY: Springer (Der Fahrzeugantrieb).

[16] Heywood, John (1988): Internal Combustion Engine Fundamentals. 1. Aufl.: McGraw-Hill Science/Engineering/Math.

[17] Dehong, Zhang; Hill, Philip G. (1996): Effect of swirl on combustion in a short cylindrical chamber. In: Combustion and Flame 106 (3), S. 318–332. DOI: 10.1016/0010-2180(95)00256-1.

[18] Masahiko Fujimoto, Kohei Iwai, Motoshi Kataoka, Michihiko Tabata (2002): Effect of combustion chamber shape on tumble flow, squish-generated flow and burn rate. In: Society of Automotive Engineers of Japan, Inc.

[19] Tippelmann, Götz (1977): A New Method of Investigation of Swirl Ports. In: SAE Technical Paper Series. DOI: 10.4271/770404.

[12] Corberán, J. and Pérez, R., An Alternative Technique for Swirl Measurement, SAE Technical Paper 980486, 1998, doi:10.4271/980486.

[21] Li, Y., A New Estimation of Swirl Ratio from Steady Flow Rig Testing, SAE Technical Paper 2014-01-2587, 2014, doi:10.4271/2014-01-2587

[22] Paulweber, Michael; Lebert, Klaus (2014): Mess- und Prüfstandstechnik. Antriebsstrang-entwicklung - Hybridisierung - Elektrifizierung, Springer, ISBN 978-3-658-04453-4